

Cell Unexcitability and Electrotonic Coupling Phenomenon Analysis of Ablation-Created Lesions: A Study Case with Ablated Explanted Human Heart

J Siles¹, J Salinet¹, CJ Crowley², F Fenton², N Bhatia³, S Iravanian², I Uzelaç²

¹ HEartLab, Federal University of ABC, São Bernardo do Campo, Brazil

² Georgia Institute of Technology, Georgia, USA

³ Emory University Hospital, Georgia, USA

Abstract

This study investigates the effects of radiofrequency ablation (RFA)-created lesions on an explanted human heart in wedge preparation by simultaneous endo and sub-endo optical mapping. The heart in Langendorff perfusion was ablated under 40 W. The ventricle was stained with Vm sensitive dye Di-4-ANBDQPQ and two excitation light bands of different penetration depths were used (red = 660 nm, green = 525 nm) to perform a conduction velocity (CV) difference analysis for identification of CV alternans. The relative change in fluorescence ($\Delta F/F$) traces were analyzed before and after ablation. Local activation time (LAT) was determined by the 50% approach. Local CV was obtained using the circle method, and RFA created lesions were characterized by examining the CV alternans correlated with transmural heterogeneities. The presence of CV alternans results from reduced excitability in a non-homogeneous lesion consisting of excitable and non-excitable cells. The absence of CV alternans in optical mapping with green light and their presence with deep-red light illustrates incomplete ablation across the ventricular wall or non-homogeneous ablation in the mid-myocardial layer. The presence of an intramural scar impairs the efficacy of the RFA procedure, suggesting a need for alternative ablations strategies.

1. Introduction

Atrial fibrillation (AF) is the most common sustained cardiac arrhythmia, affecting 2.9% of the worldwide population [1]. AF is associated with significant hemodynamic and thromboembolic complications [2]. In comparison, ventricular tachycardia (VT) usually occurs in structurally diseased hearts. Radiofrequency catheter ablation (RFA) is currently the most effective invasive treatment for the termination and prevention of AF and VT re-occurrence, creating tissue lesions through thermal injury. The geometry of the lesion profile is postulated on predefined profile

of heat transfer in homogeneous tissue. However, factors such as catheter pressure force, catheter-tissue impedance, the ground patch's location, and most importantly tissue heterogeneity such as the presence of fibrotic tissue affect the lesion profile. For example, the common RFA strategy for VT is to identify a clinically relevant scar tissue and deliver ablative energy to homogenize the scar. However, the effects of RFA on fibrotic tissue are not fully understood [3]. Conduction velocity (CV) slowing is one of the determinants for AF and VT vulnerability [4]. One of the mechanisms leading to arrhythmia due to CV slowing is reentry formation [5]. This occurs when a reentrant wave encounters an excitable tissue recovered from its refractory phase, if the propagating time around the block zone is longer than the refractory period [6]. To quantify CV slowing, it is important to identify CV changes at the high spatiotemporal resolution across the myocardium, and also across myocardial wall, to identify and characterize regions of delayed activation for a better understanding of the mechanism leading to arrhythmia. Conduction velocity is altered in failing hearts and it depends on fiber direction, tissue heterogeneity such as trabeculated or fibrotic tissue, age, presence of local ischemia, and inflammation factors. Optical mapping directly measures transmembrane action potential (AP) at a high spatial resolution, achieving sub-millimeter mapping density. Therefore, it is a method of choice in basic science research to study cardiac electrophysiology from cells to tissue and whole heart level. In this study, we investigated the effect of RFA on the profile of created lesions on an explanted human heart in wedge preparation by simultaneous endo and sub-endo optical mapping by analyzing CV alternans using excitation light bands of different penetration depths to estimate the lesion depth across the ventricular wall.

2. Methods

The explanted human heart was obtained through the Emory Hospital Heart transplant program under the Institute Review Board (IRB) approval from heart transplant re-

ipient undergoing heart transplantation and with the consent of the patient.

2.1. Human heart preparation and wedge preparation

In a heart transplant procedure, a surgeon extracted the diseased heart. Immediately afterward, ice-cold cardioplegia solution was flushed through the right and left coronary arteries to reduce myocardial oxygen demand by creating electrical quiescence and cooling the heart to reduce the ischemic effects during transportation, up to 30 minutes, to the optical mapping laboratory. Optical mapping was performed on the left ventricle endocardium in a wedge preparation. The left marginal artery was cannulated, and the cannula was secured with a surgical silk ligature. Leaks around the tissue edges were secured by clamping around the cut section to maintain adequate coronary pressure of 70 mmHg with a flow rate between 10 and 20 mL/min (Figure 1A). The wedge preparation was placed in an oval heated chamber maintained at 37°C and perfused with oxygenated Tyrode solution composed of (in mmol/L): 128.2 NaCl, 4.7 KCl, 1.19 NaH₂PO₄, 1.05 MgCl₂, 1.3 CaCl₂, 20.0 NaHCO₃, and 11.1 glucose, and gassed with 95% O₂-5% CO₂; pH=7.35 [7]. The heart motion was suppressed with (-)-Blebbistatin (Cayman Chemicals) at 1.8 μM concentration in Tyrode perfusate. Then, the ventricular tissue was ablated using a non-irrigated tungsten electrode for duration of 20 seconds and radiofrequency power set to 40 W using a high frequency desiccator (Bovie Derm 942, Bovie).

2.2. Optical mapping process

For the optical mapping measurements, the transmembrane voltage (Vm) sensitive dye Di-4-ANBDQPPQ (JPW-6003) was prepared as a stock solution previously dissolved in pure ethanol at a 1 mg/mL ratio, and a total of 0.5 mg of the dye was used for the wedge preparation.

Two red LEDs (660 nm) and two green LEDs (525 nm) were used as the dye excitation sources in alternating sequence (Figure 1A). The red LED light was collimated with a plano-convex lens (ThorLabs) and bandpass filtered with a 660/10 mm filter (Edmund Optics). The green LED light was collimated with a plano-convex lens (ThorLabs) and bandpass filtered with a 520/10 mm filter (Edmund Optics). A custom-designed two-channel LED driver was used, with the ability to switch the excitation light bands in sync with the camera frame rate (donated from Aleksa Tech). The emitted fluorescence was passed through a 700 nm long-pass filter (Chroma) on the camera side. The sequence of images was acquired at 500 Hz using an EMCCD camera (Evolve 128, Photometrics) at a resolution of 128 × 128 pixels.

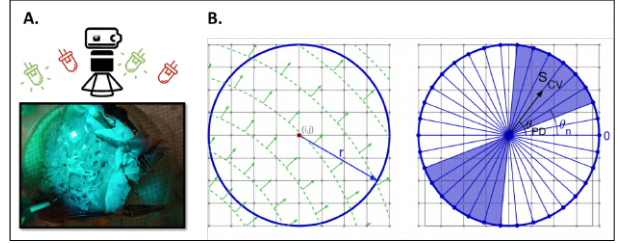


Figure 1. A. Representation of the optimal mapping setup, presenting the excitation sources (two red deep LEDs and two green LEDs) and the EMCCD camera; B. Illustration of the circle method. At right, LATs differences at the points along a circle of radius r , centered at a grid point (i,j) . At right, an example of a wave propagating at 45° with a set of test CV values as a difference in LATs along diameters (blue lines) at different angles θ_n . The geometrically weighted average of $S(\theta_n)$ over an angular range around θ_{PD} is represented by the blue shaded region

2.3. Post-processing

The baseline drift for each pixel trace was removed by applying a low-pass Kaiser Window FIR filter with a stop-band frequency of 1 Hz and a pass-band frequency of 0.5 Hz. The output signal from the FIR filter, representing the baseline drift, was subtracted from the raw pixel trace. The difference was divided with the baseline drift signal, obtaining the relative change of fluorescence $\Delta F/F$ [8]. To boost Signal to Noise Ratio (SNR), approximately 40 optical APs (OAPs) were stacked (ensemble-averaged) with a period equaling two beats upon reaching steady-state conditions, significantly reducing the noise [9]. In the next step, the traces were temporally filtered using an anisotropic 1D diffusion filter [10], which preserves the OAP upstroke.

Local Activation Times (LATs) were obtained by linear fit along the OAP upstroke and determining the 50% rise of the OAP upstroke. As the sampling rate is generally lower with optical mapping, the first derivative method is less accurate than the 50% approach. Obtained LAT maps were minimally filtered using an anisotropic 2-D diffusion filter, which preserves sharp boundaries in LAT maps [10].

2.4. Circle Method (CM)

CV was calculated applying the circle method (radius = 3 pixels), presented in a previous study [11]. Assuming a planar wavefront propagation inside a circle of radius r (Figure 1B), centered around each LAT grid point, the CV can be determined as follows. First, differences in the LAT across the endpoints of chords passing through the circle's center are calculated. Then, from the LAT differences, an

effective conduction speed, $S(\theta)$, can be calculated as a function of the chord's orientation angle, θ . The maximum of $S(\theta)$ corresponds to the true conduction speed along the propagation direction, $S(\theta_{PD})$. The evaluation of $S(\theta_{PD})$ incorporates measurements along a single path, centered at the LAT grid point. CV along neighboring chords can be incorporated to reduce the effect of LAT measurement uncertainty.

To reduce noise in the determination of the CV, a range of conduction speeds is combined to calculate a CV that is spatially averaged over the blue area subtended by the chords (Figure 1B right). The resulting conduction speed can be calculated from the average of these back-projected speeds as,

$$S_{CV} = \frac{1}{N} \sum_{n=1}^N \frac{S(\theta_n)}{\cos(\theta_{PD} - \theta_n)} \quad (1)$$

for all N chords lying within the range spanned by $\Delta\theta$. Finally, using the CV maps calculated, the relative CV (ΔCV) was obtained as a relative difference in CV before and after ablation for each of the two excitation bands and separately for even and odd beats.

3. Results

Figure 2 shows LAT maps from optical mapping measurements on the explanted human heart with endocardial ablation using green and red light excitation bands, and the LAT map before the ablation (baseline). The baseline LAT maps obtained with either green or red light excitation are statistically the same. The second row shows corresponding CV maps. The ΔCV difference maps were not practical to characterize RFA-lesion due to highly non uniform CV maps (RFA - baseline). The last row shows the ΔCV calculated as a relative difference between even and odd CV maps after the ablation for the green light (left) and red light (right) excitation bands. The colorbar range in all figures was set from the 5th to 95th percentile, except for ΔCV maps where the upper boundary was set to zero.

Analysis of relative difference CV maps for subsequent beats with green light excitation does not show the presence of CV alternans, indicating a complete surface ablation. However, the same analysis with red light excitation of deeper tissue penetration shows CV alternans due to incomplete or non-homogeneous ablation across the ventricular wall. This observation agrees with the photos of the RFA-lesion taken after the experiment (Figure 3A), showing the spatial extent of the lesion and its depth across the ventricular wall (Figure 3B).

4. Discussion

One of the challenges in ventricular tissue ablation is depth estimation of the created lesions. In this study, we

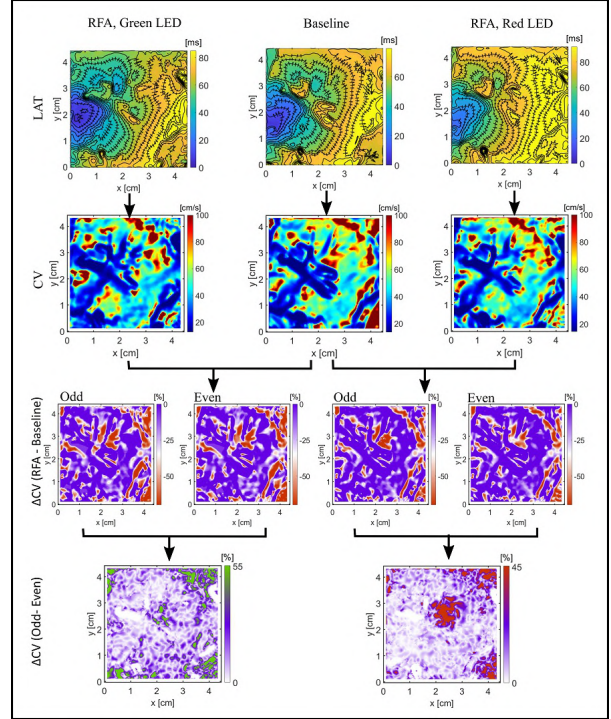


Figure 2. Optical mapping on the LV's endocardium in wedge preparation for quantification of RFA-created lesion. LAT maps for baseline, using red LEDs and green LEDs. Then, the CV maps and the ΔCV as a difference between before and after ablation for subsequent beats (Odd and even). Finally, the ΔCV maps between Odd and even

used two different light bands for excitation of the V_m dye, a green band centered at 525 nm and a deep red band centered around 660 nm, for optical mapping of the human endocardium. Tissue penetration depth is generally under 1 mm for green light, and over 3 mm for deep red light [12]. Two different light bands enable us to study the differences in the CV maps obtained from AP signals emanating from the surface layer and AP signals from the deeper layers (Figure 2 bottom). As human endocardium is highly trabeculated, and in addition the presence of papillary muscle results in a highly heterogeneous, a resulting CV map is highly non-uniform hindering the ablated area as the zone of decreased CV. Amplitude alternans, the beat-to-beat variation in AP amplitudes, occur as a result of decreased excitability such as when cardiac cells are coupled with scar tissue. Therefore, to quantify RFA lesions, CV alternans maps are more suitable than CV maps. As shown in Figure 3B, the depth of the created lesion is 3 - 4 mm. Corresponding optical AP traces from the surface layer of the lesion with green light excitation are solely due to electrotonic coupling between un-excitabile cells, resulting in no alternans present at a slow pacing cycle length

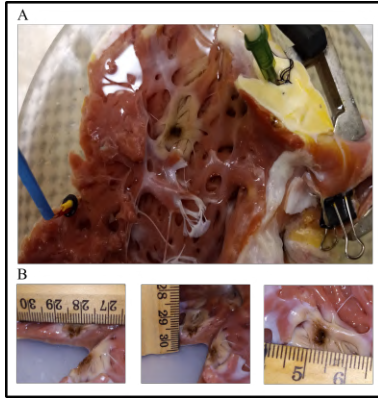


Figure 3. A. Endocardial tissue after the RFA; B. Ablation lesion size (5 x 5 mm) and depth (3 - 4 mm)

(PCL) of 800 ms. However, deep red light excitation shows the presence of CV alternans due to incomplete transmural ablation due to heterogeneous volumes of excitable and non-excitable cells. For example, one mechanism leading to CV alternans could be due to the presence of unexcitable cells coupled with excitable cells resulting in the reduced cell-to-cell coupling, leading to decreased excitability.

5. Conclusion

The effect of RFA on a lesion profile using an explanted human heart in wedge preparation was quantified with excitation light bands of different penetration depths to estimate lesion depth across the transmural wall. Presence of CV alternans at slow PCL indicates reduced cell to cell coupling and was characteristically present in the ablated region with red light band excitation and absent with green light band excitation. While optical mapping is limited to lab research, its high spatial resolution enables quantification of tissue heterogeneity at a sub-millimeter scale, useful to characterize heterogeneous scar tissue often responsible for VT due to the presence of micro-reentrant pathways. In contrast, low spatial resolution of contemporary electroanatomical mapping systems is severely limited to characterize scar tissue and tissue conduction heterogeneity. With the optical mapping approach, new insights may help to better understand arrhythmia mechanisms and RFA effects on tissue electrophysiology to develop improved ablation strategies.

Acknowledgments

J. Siles is supported by grant #2020/03601-9, São Paulo Research Foundation (FAPESP) and the Program of Alliances for Education and Training (OEA-GCUB-2017). I. Uzelac and J. Salinet are supported by grant #2018/25606-2, São Paulo Research Foundation

(FAPESP). This study was also supported in part by the NIH under grant 1R01HL143450-01, and the NSF under CMMI-1762553.

References

- [1] Benjamin EJ, et al. Heart disease and stroke statistics–2019 update: A report from the American Heart Association. *Circulation* 2019;139(10):e56–e528.
- [2] Zimerman L, Fenelon G, Martinelli M. *Diretrizes Brasileiras de Fibrilação Atrial*, volume 92(6 supl. 1). Arq Bras Cardiol: Sociedade Brasileira de Cardiologia, 2009.
- [3] Scanavacca MI, Sosa E. Catheter ablation of atrial fibrillation: Techniques and results. *Arquivos Brasileiros de Cardiologia* 2005;85:295–301.
- [4] Narayan SM, et al. Repolarization alternans reveals vulnerability to human atrial fibrillation. *Circulation* 2011; 123(25):2922–2930.
- [5] Nattel S, et al. Mechanisms of atrial fibrillation: lessons from animal models. *Progress in Cardiovascular Diseases* 2005;48(1):9–28.
- [6] Spector P. Principles of cardiac electric propagation and their implications for re-entrant arrhythmias. *Circulation Arrhythmia and Electrophysiology* 2013;6(3):655–661.
- [7] Ng FS, et al. Adverse remodeling of the electrophysiological response to ischemia–reperfusion in human heart failure is associated with remodeling of metabolic gene expression. *Circulation Arrhythmia and Electrophysiology* 2014; 7(5):875–882.
- [8] Uzelac I, Irvanian S, Fenton FH. Parallel acceleration on removal of optical mapping baseline wandering. In 2019 Computing in Cardiology (CinC). IEEE, 2019; Page–1.
- [9] Uzelac I, Fenton F. Robust framework for quantitative analysis of optical mapping signals without filtering. In 2015 Computing in Cardiology Conference (CinC). IEEE, 2015; 461–464.
- [10] Perona P, Malik J. Scale-space and edge detection using anisotropic diffusion. *IEEE Transactions on Pattern Analysis and Machine Intelligence* 1990;12(7):629–639.
- [11] Siles-Paredes JG, et al. Circle method for robust estimation of local conduction velocity high-density maps from optical mapping data: Characterization of radiofrequency ablation sites. *Frontiers in Physiology* 2022;13.
- [12] Avci P, et al. Low-level laser (light) therapy (lllt) in skin: stimulating, healing, restoring. In *Seminars in cutaneous medicine and surgery*, volume 32. NIH Public Access, 2013; 41.

Address for correspondence:

Jimena Gabriela Siles Paredes
 Biomedical Engineering - CECS
 Federal University of ABC - UFABC
 Street: Av. Anchieta, Sao Bernardo do Campo - SP, Brazil
 E-mail: jimena.gabriela@ufabc.edu.br